Shape and size transformations of biomass particles during combustion

Shape and size transformations of biomass particles during combustion

Juan Riaza[1], Patrick Mason[2], Jenny M. Jones[2], Alan Williams[2], Jon Gibbins[1, 3], Hannah Chalmers[1*]

1 Institute for Energy Systems, School of Engineering, University of Edinburgh. The King's Buildings, Mayfield Road, Edinburgh, EH93JL, Scotland, UK

2 School of Chemical and Process Engineering, University of Leeds, Leeds, LS2 9JT

3 Department of Mechanical Engineering, University of Sheffield. Mappin Street, S13JD, Sheffield

Abstract

Combustion of individual particles of different woody and agricultural residue biomass have been studied under a laboratory scale rapid-heating apparatus. Particles used were in the size range of 300- 1400 mm and weight 0.5-7 mg. A wire mesh element is used to radiatively heat the particle to 1200-1400K. The apparatus allows a high-speed camera to record the combustion of the individual particles directly. Examination of the resulting video images showed a sequential combustion of volatile matter followed by burn-out of the remaining char for all fuels. Analysis identified differences and patterns in burnout time, combustion behavior and the evolution of char size and shape transformations.

Heterogeneous behavior was observed between the different biomass samples and also among particles within some of the samples. Particles with initial prolate (fibrous) shapes have been observed to become more equant (quasi-spherical) during combustion. Measurement of the particle dimensions during its combustion extracted from the images of the high speed recording have allowed evaluation of the size and shape changes to be mapped. Particle size and shape appears to change only slightly during devolatilization and swelling was rarely observed. Following devolatilization, during the remaining char

combustion, more pronounced changes in the size and shape of the particle are apparent. In most cases the shrinking char becomes more rounded as the char particle partially melts and contracts due to surface tension. This transformation is more distinct in some of the biomass samples. Profiles and images of the different fuels examined are presented.

Keywords: combustion, biomass, char shape

** Corresponding author:*
e-mail: hannah.chalmers@ed.ac.uk
Tel: +44 (0)131 6507444, fax. +44 (0) 1316506554

HIGHLIGHTS

- Combustion of single particle of five different biomass fuels
- Thermal imaging camera was used during combustion
- Biomass char shape and aspect ratio was calculated during combustion.
- During char combustion, particle shape changes from elongated (prolate) to spheroid (equant) are observed

1. Introduction

Biomass power plants can provide large scale reliable energy with the flexibility to meet potentially unpredictable electricity demand. Biomass power is classed as a renewable source and is a key option for achieving a low-carbon electricity supply while meeting environmental targets on emissions and renewable energy. Many different biomass sources have been studied as fuels with a wide range of physical and chemical properties. The standardization of biomass fuel in the form of high energy-density pellets allows easier management and more sustainable transport to all scales consumers [1]. This also facilitates reliable performance of combustion plant with less variable ash content and calorific value of the fuel. Large power plants such as Drax and Lynemouth in the UK have opted for high quality biomass pellets to minimize problems in the combustion process. However this high standard on biomass fuel quality makes it also more expensive. A more diverse range of source materials will benefit with lower prices. However, lower quality fuels present technological challenges for biomass power plants in maintaining combustion efficiency, avoiding ash fouling issues and complying with strict pollutant emissions limits. Overcoming these challenges will enable better use of limited biomass resources such as new biomass fuels, from energy crops and residues.

Single particle combustion (SPC) devices are relatively simple experimental apparatus that can provide reliable information to study the main variables that affect combustion kinetics and compare different fuels combustion behaviour [2, 3, 4, 5, 6]. Biomass has high volatile matter content, less carbon, more oxygen and a lower heating value than coal. Moreover, due to higher reactivity of biomass, a bigger particle size range can generally be used for biomass fuels compared with pulverized coal. Previous studies on single particle device, provided an approximation to milling requirements for biomass fuels in terms of maximum particle size for efficient burn-out [7, 8]. Other single particle studies have identified the differences

between different fuels behaviour during combustion [7, 3, 8, 9], providing details on ignition [10, 11, 12, 13], volatile flame [14], char combustion [15], particle morphology [16], combustion atmosphere [17,18] or temperature [8, 18]. Flower et al. [5] conducted biomass single particles studies in a wire mesh single particle setup for particles between 5 and 30 mg and showed relatively low dependency on the aspect ratio of the samples. Mason et al. [3] performed a series of single particle experiments which identified useful empirical functions to describe the relationship between particle size and burnout time, allowing the behaviour of different fuels in a furnace to be compared.

Biomass shows significant differences in ignition and combustion temperatures and burnout times [2]. The observations made on small scale lab combustion produce relevant information on the combustion behaviour for comparison among different fuels. This information together with other parameters can be used for computer fluid dynamics (CFD) modelling of the combustion process at any scale. CFD has been increasingly improving the resolution of the combustion process modelling in recent years, providing better prediction results for new developments. This has enabled lower pollutant emissions such as NO_x reduction [19] to be achieved through optimised process design.

The shape, size and density of the particle is important for fluid dynamic modeling as it can affect the trajectory and residence time of the fuel particle inside the boiler [20]. Large particle size implies ignition delay [21] and longer burnout time [3,7], and therefore higher amount of carbon in ash in a furnace. The monitoring and control of fuel particle size distribution is important to achieve a complete and efficient combustion. Panahi et al [21] reported on recent studies the spheroidation of elongated biomass particles with an initial aspect ratio between 4 and 8 becoming almost spherical during pyrolysis. This spheroidation is explained because measured temperatures during volatile mater combustion are higher than

98 the melting point of main biomass components as cellulose (732- 739 K). They also
99 concluded higher aspect ratio leads to faster ignition. Bonefacic et al [20] analyzed the
100 influence of the geometry of particles in the combustion process. Their model revealed that
101 particle geometry has a significant impact on the starting point and the rate of devolatilisation
102 as well as the char burning. Higher aspect ratio of the particles leads to increased scattering of
103 fuel, accelerating the devolatilization process and enhancing the mixing of volatiles with the
104 air. Yang et al. [22] developed a mathematical model that predicts the behavior of a range of
105 particles of different sizes, demonstrating the occurrence of the general features of
106 combustion and the occurrence of a combustion wave. It explained the differences observed
107 between spherical and cylindrical biomass particles. These observations are consistent with
108 experimental observations made by same authors using suspended biomass particles and
109 other works in the literature. Gubba et al [23] validated a CFD model including different
110 particles shape distribution and found significant influence of the internal thermal gradients
111 on the surface temperature, residence time and combustion performance. Momeni et al [24]
112 also studied shapes and size effect on combustion process of single biomass particles,
113 cylindrical particles were found to lose mass faster than spherical particles and the burnout
114 time was shortened by increasing the particle aspect ratio (surface area). Similarly, Lu et al
115 [25] obtained differences during devolatilization depending on the shape of the initial
116 particle. The conversion times of cylindrical particles with almost the same surface
117 area/volume ratio are very close to each other.
118 It is clear from the literature, that assuming that fuel particles are approximately spherical is a
119 reasonable approach for modeling some solid fuels like coal, obtaining good agreement with
120 experimental results [26, 27]. However this assumption is generally not enough for
121 lignocellulosic biomass which tends to have elongated particle shapes. The model developed
122 by Yang et al. [22] predicts a change on particle shape. However more detailed experimental

data in the literature on the evolution of particle size, shape, or temperature changes during combustion of different biomass fuels is needed.

Combustion experiments on a single particle combustion apparatus have been undertaken using various biomass materials with the objective of evaluating the differences among particles of different biomass fuels on their combustion; including volatile burning time, char combustion time, particle temperature and adding new information regarding particle size and shape changes. The dimensions of the particle during combustion have been measured providing precise novel data regarding shape and size changes during combustion of different biomass materials. The study examined a range of biomass and different particle sizes compare times required for burnout for the different fuels. The information provided by the video observation can also provide fundamental data for other researchers developing new models to more accurately describe the changes in particle size and shape during combustion process at a particle level.

2. Materials and methodology

2.1. Fuel samples used

A series of experiments have been made with five different biomass samples. The biomass sample used were pine (PI), eucalyptyus (EU), willow (WI), olive waste (OW) and steam exploded wood ('black') pellet (BP). Each fuel was characterized in terms of chemical composition by proximate analysis, ultimate analysis, and gross calorific value. Results are presented in Table 1.

Table 1. Proximate and ultimate analysis of the samples used.

		Pine	Eucalyptus	Willow	Olive residue	Black pellet	Basis	units
Proximate Analy	moisture content	8.3	8.1	3.1	5.9	7.2	as received	%wt

	ash content	2	0.9	2	7.6	4.2	d.b.	%wt
	volatile content	80.85	82.55	81.93	74.01	76.07	d.b.	%wt
	fixed carbon	17.15	16,55	16.07	18.39	19.73	d.b.	%wt
	GCV (dry)	18.6	19.4	19.8	20.1	20.0	d.b.	$MJ.kg^{-1}$
	Particle density	0.48	0.67	0.52	1.3	1.26	d.b.	$mg.mm^{-3}$
Elemental Analysis	C	46.45	48.76	49.78	48.79	50.49	d.b.	%wt
	H	5.19	5.55	5.88	6.01	5.56	d.b.	%wt
	O	44.98	44.69	41.85	36.13	39.47	d.b.	%wt
	N	1.27	0.1	0.39	1.48	0.19	d.b.	%wt

Each sample was milled, dried and sieved to obtain different ranges of sizes

The particle size ranges used for the experiments were 300--1400 μm. These sizes were selected to be high enough to have meaningful images for the shape analysis and targeting with the thermal imaging camera while being small enough to enable the assumption of uniform particle temperature (i.e. thermally thin). This upper range is also representative of the largest size fraction that would typically be used in a pulverized fuel boiler. Samples were dried in an oven at 115 ºC for 2 hours to remove any moisture before combustion experiments in the wire mesh reactor.

2.2. Experimental device

The experimental device used at the University of Edinburgh has been previously described at [7]. The wire mesh reactor (WMR) apparatus used in this work allows a stationary particle sample to be recorded with high speed video camera as it burns. The reactor was based on the WMR used by Flower et al. [5], and is shown schematically in Figure 1. The particle under test is supported between 2 vertical wire meshes that heat the particle by radiation, which is consistent and permits reproducible results. The electrical current through the elements can heat them to their operating temperature within 500 ms, which is small compared to particle burning times. The output current was limited to enable an operating mesh temperature of 900 ºC, and estimated heating rate of ~10^3 ºC s-1. The reactor temperature was measured with

166 an k-Type thermocouple centred between the two meshes to ensure that the heat flux was
167 consistent between runs, permitting valid particle-to-particle comparisons. The sample holder
168 was placed on the centre line between the meshes The sample holder was made of the same
169 wire mesh material as the heating elements, forming a rectangle of 3 x 6 mm to place the
170 sample over it. The effect of mesh heating rate and final temperature affects the particle
171 ignition delay, but once the particle ignites the heat coming from the combustion becomes the
172 main source of energy for the particle temperature. Small errors on the mesh temperature
173 will, therefore, have little effect during the combustion performance and burnout time.
174 The high speed camera used in this study was a Phantom Miro eX4 with a zoom lens coupled
175 to a 20 mm expansion tube to give image magnification. It was placed on the top of the
176 apparatus. The camera-to-particle distance was fixed so that a consistent optical
177 magnification was achieved. The high speed video recording allowed a good temporal
178 resolution to be achieved. 500 frames per second were normally used for the recording
179 exposure time of 3300 μs and resolution 128X128 pixels. A PC was used to retrieve the
180 images from the camera and all the videos were analysed using Phantom Control Camera.
181 The recording was played back in real time and at reduced speed, allowing observation of
182 much smaller particles and also phenomena that would be missed with a normal camera. The
183 times for the respective phases in particle combustion were then accurately determined by
184 processing the video image files and representative rankings of burning times were obtained.
185 All particles were weighed before the experiment and the burnout time for each particle could
186 be measured from observation of the video.

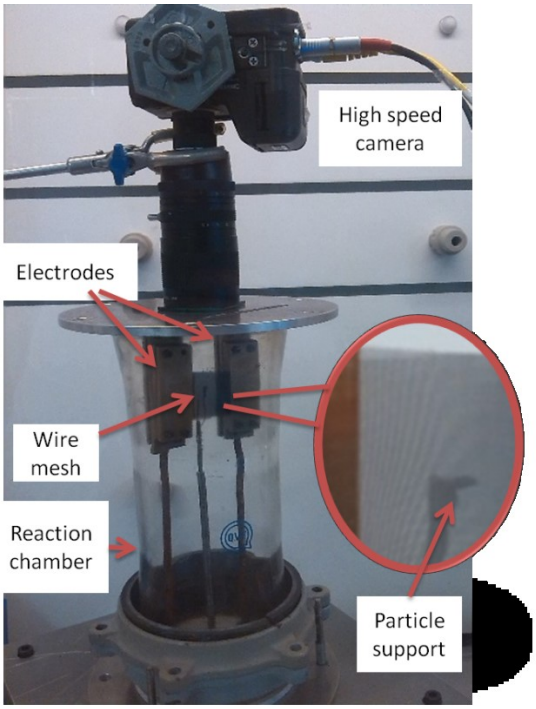

Figure 1. Single particle experimental setup.

2.3. Thermographic imaging

Measurement of the surface temperature of the combusting particle was possible by use of thermal imaging. In this study, a FLIR A600 series infra-red thermographic camera was used for this purpose. This camera has a focal-plane-array thermal detector with a measurement range up to 2273K and sensitivity specified as 0.05K with an accuracy tolerance of 2% of reading (i.e. ±30K at 1500K).

The images are derived from the intensity of the infra-red radiation detected by the thermal detector in the camera. The temperature of the particle's surface can be derived from the data although it is necessary to account for the emissivity of the surface. An emissivity of 0.85 was adopted for the entire range of the combustion process being observed with thermal imaging based on reported values for biomass char [28]

3. Results and discussion

3.1. Ignition and combustion behaviour analysis

All biomass fuels studied presented a sequential combustion with two well differentiated stages, volatile flame and char combustion. This is in agreement with previous works completed with this, and other single particle devices [2,3,4,7]. Upon ignition, the gases released through the pores of the particle created a smooth volatile flame surrounding the particle. This volatile flame became bigger and increasingly luminous and then shrinks to extinction. Char ignition follows until completion of particle char burnout. Figure 2 shows images from the videos of all biomass samples examined at different stages of combustion. Video files can be found on supplementary material section. In order to measure the burnout times and compare between the different tests, 0% burnout is the last frame before visible ignition takes place and 100% the first frame where there is not any visible combustion at all. The brightness and contrast of the images at 0% burnout were adjusted in order to have a clearer image of the original particle. It is noted that OW was especially difficult to distinguish from the background support so the particle perimeter is underlined in blue in the first image.

3.1.1. Ignition delay

The delay between the start of heating to particle ignition is very consistent between the different runs and different samples. However the delay can increase significantly with higher moisture content, as observed by previous studies [3].

3.1.2. Devolatilisation

After heating and drying, the pyrolysis reactions start to take place and they continue until a stable char is formed. In fast pyrolysis, biomass decomposes very quickly generating mostly gas, vapours, aerosols and char. The biomass pyrolysis starts releasing light hydrocarbons and main products such as H_2, H_2O, CO, CO_2, and CH_4. These products start the ignition of the volatile flame. The biomass particles appeared to start releasing volatiles a

few milliseconds before ignition, this was visible on the images of the olive waste which produced a blurry image and darkening on the surroundings of the particle. Nevertheless, the ignition delay time is negligible in respect to the overall burnout time.

All samples showed homogeneous ignition and no significant differences were observed in the volatile flame development. As the temperature increases, biomass fuels decompose into primary volatiles. At temperatures above 773 K, the primary volatiles are subject to a secondary pyrolysis, during which the tars are converted into a variety of gaseous species, especially CO, light hydrocarbons, hydrogen and CO_2. The pores of the particle become open and connected after a mass-loss front (moisture evaporation or devolatilisation) propagates from the particle interior [22]. The gases from pyrolysis reactions flow through the porous medium inside the particle reaching the surface and creating the volatile flame around the particle. As the pyrolysis completes, the volatile flame shrinks as can be noted on the images for WI and PI comparing 25% and 45% burnout images on Figure 2. As the outward flow of pyrolysis products reduces, the oxygen reaching the solid surface increases and char ignition is initiated.

There are notable differences between the samples regarding the times required for volatile burning. The composition of biomass, the amount of volatiles and the pyrolysis kinetics of each biomass, affects the duration of the volatile flame. Average volatile/char burning percentages are presented in Figure 4. As shown on Figure 2, at 25% the video shows the volatile flame surrounding the contour of the biomass particle very clearly in the case of EU, PI and WI. In the case of BP the particle is in transition to char ignition, while the OW particle shown in the figure has already completed the volatile combustion stage and the remaining char particle has ignited at one end of the particle.

The EU particles had the most elongated shaped particles. Given that, it was observed that the volatile flame in the centre of the particle and char ignition on both ends of the particle

overlapped for a few milliseconds. On the contrary, BP sometimes exhibited a few milliseconds delay between the volatile flame extinction and the complete ignition of the char. This is not the case on the BP particle on Figure 2 at 25% where there is still some blurriness due to the end of the volatile flame while the char particle on the background has already ignited.

WI and PI continue showing volatile flame at 45% burnout, and even at 60% burnout the WI particle shows a small volatile flame while the char has completely ignited.

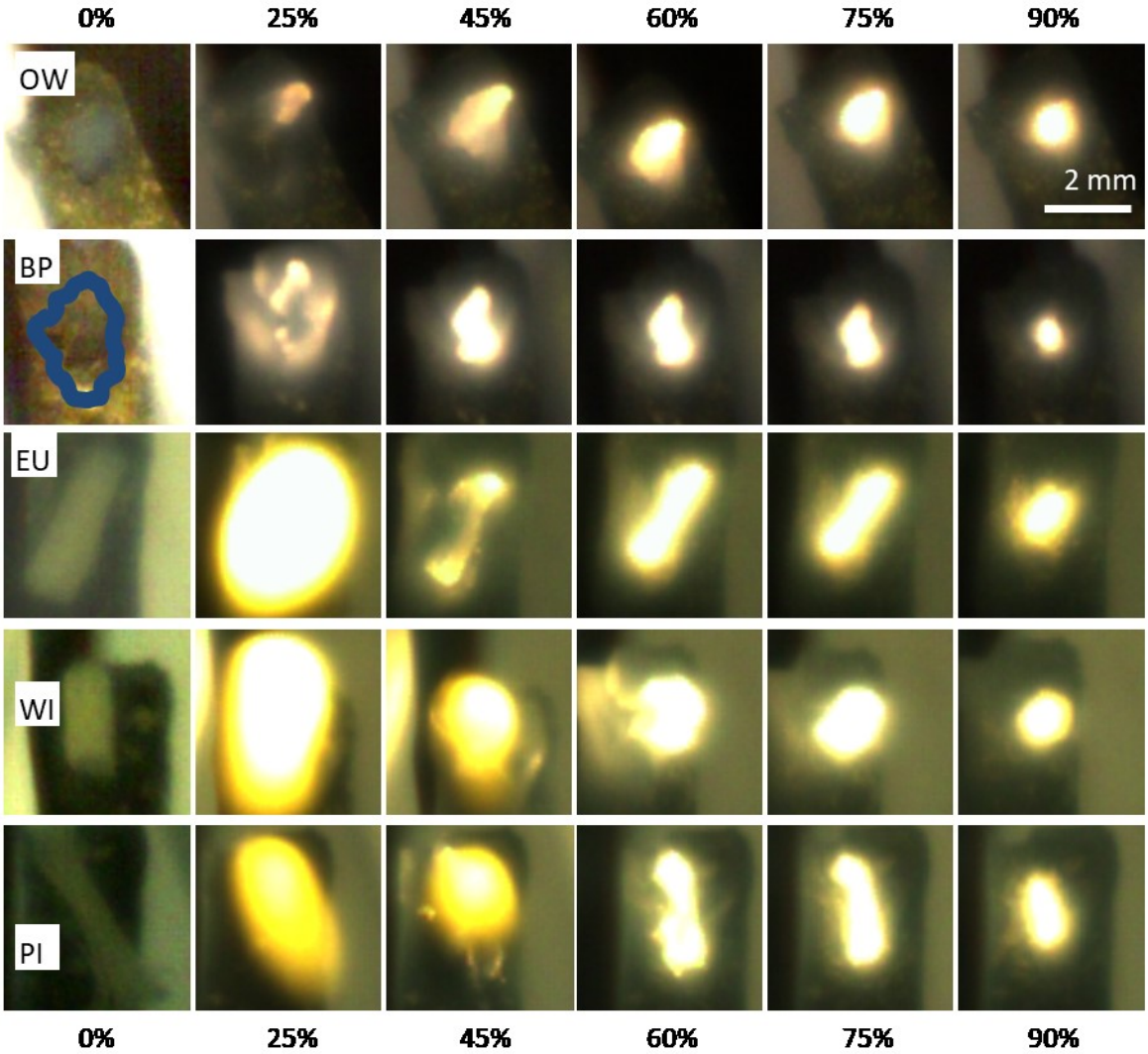

Figure 2. Images from the combustion recording of: olive waste (OW) steam torrefacted wood pellet (BP), eucalyptyus (EU), willow (WI) and pine (PI) particles at different percentages of burnout time.

3.1.3. Char combustion

For some cases the flame front could be observed during particle char ignition. Comparing OW particle at 0% and 45% burnout in Figure 2, it can be observed that the particle moved or changed during the devolatilization stage. In this particular case, the particle just rolled over the support. Changes were occasionally observed with deformations and bending of some particles. Swelling has also been observed in some cases; however there was not a significant number of swelling cases at the volatile burning stage for any of the samples tested to quantify this. The majority of them remain unchanged or shrink slightly on the major axis (length). An increment in the size of the particle was observed on the minor axis (width) in some particles during devolatilization. Rather than swelling, as some bituminous coals do, this phenomenon can be attributed to the separation of fibres of the particle. Images from the char at the different stages of combustion evidenced particle shape changes. The observartions of particle shape and projected area evolution observations are addressed in detail in section 3.4.

At the end of the particle combustion the ash remains incandescent over the support for a few milliseconds before cooling down. It is observed that the ash distributed all over the particle is transported during char combustion. While the particle is consumed the ash reaches the particle surface. In some of the particles, the ash creates a coarse surrounding the particle. At 100% burnout, the coarse ash remains incandescent with a shape that is proportional to the char particle on its last stage of combustion.

3.2. Burnout time for single particle combustion

Particles of different weight and sizes were evaluated through the single particle experimental device in order to study the effect of particle size on the combustion behavior of

289 the fuels as well as their burnout time. The variability on the aspect ratio of the woody
290 biomass particles makes the relationship between particle cut size and particle mass
291 imprecise. As a result, it is difficult to predict accurately a biomass particle mass for a given
292 particle cut size. Therefore this relationship needs to be taken with its limitations and results
293 are represented based on particle weight not on their size. The corresponding range size will
294 depend on roundness of each fuel particle. A significant number of experiments were done
295 with each sample on a range of weight from 0.5mg to 5 mg. Some experiments were done
296 with particles above 5 mg in order to ensure the trends obtained are in agreement with
297 previous results [3, 5, 7] The particle weight versus burnout time for each particle of the
298 different biomass tried is plotted in Figure 3. The deviation of the trend is large for some of
299 the particles also because the heterogeneity of biomass particles composition.

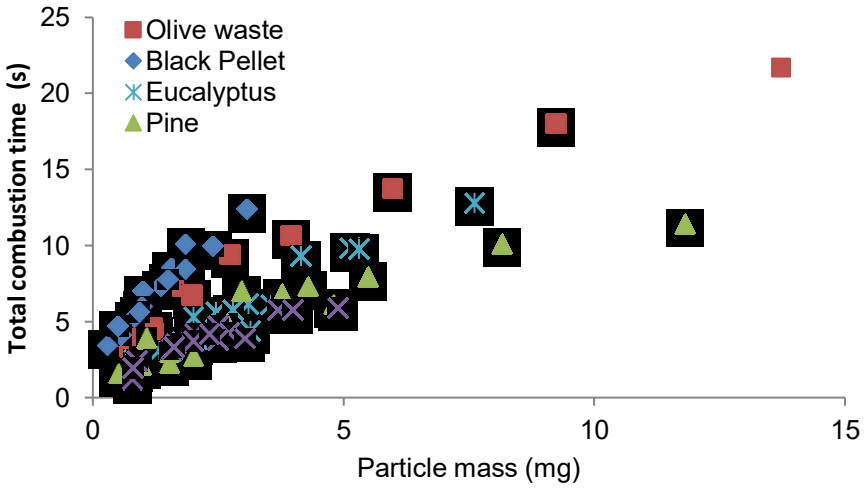

300

301 **Figure 3. Burnout time obtained for different biomass samples**

302 The burnout time increase with the increment of particle weight for all samples. The
303 relationship between weight and burnout time results for biomass particles were consistent
304 with that observed in previous SPC studies [3] where the data could be fitted to a regression
305 function of the form $t=a.mass^b$ where a and b are empirically derived coefficients. In this
306 study, the best adjustments were obtained for a second order polynomial function. Equations
307 and R^2 values are represented on Table 2. The burnout time trend lines versus particle mass

cannot be directly transposed to large scale conditions burnout times, as the heat transfer and combustion conditions are different, but it provides a useful means to compare different biomass samples. For a better comparison among the samples, values for extrapolated burnout time for volatiles and char for a particle of 2 mg are plotted on Figure 4.

Table 2. Burnout time, normalized projected area and char temperature observed for the different samples

Sample	Burnout time	R2	Range	Char Temperature	Normalized Particle Projected Area	R2
BP	$t = -0.384m^2 + 4.454m + 2.11$	0.959	0.5 - 3 mg	-	$A = -79.93t^2 + 5.565t + 100$	0.965
OW	$t = -0.428m^2 + 4.34m + 0.25$	0.951	0.5 - 4 mg	-	$A = -169.49t^3 + 83.997t^2 + 19.314t + 100$	0.9864
EU	$t = -0.028m^2 + 1.857m + 0.59$	0.935	1 -7 mg	1405	$A = -88.83t2 + 8.6t + 100$	0.959
PI	$t = -0.075m^2 + 1.787m + 0.64$	0.979	0.5 - 5.5 mg	1422	$A = -271t^3 + 319t^2 - 123t + 100$	0.9593
WI	$t = -0.246m^2 + 2.43m - 0.11$	0.943	1 -5 mg	1392	$A = -115.6t^2 + 55.5t + 100$	0.981

The differences observed between samples must be attributed to the differences on reactivity of the fuels. The regression functions for WI, EU and PI were almost overlapping. WI was slightly lower, which suggests a higher reactivity, being therefore the most reactive of all samples tried. OW was notably above those. Olive waste is been reported in the literature to have lower reactivity than other biomass due to high content in lignin [29, 30]. The steam-exploded wood pellet (BP) sample showed the lowest reactivity with the longest burnout times. The raw material before torrefaction was not available to compare in this study, so the low reactivity cannot be attributed to the process of torrefaction alone. However, Jones et al [31] reported that torrefaction produced less reactive biomass chars, similarly Vorobiev et al. [32] reported that the char burnout rate was found to decrease with torrefaction intensity of beech wood. Other works by Lu et al [33] did not find differences on intrinsic reactivity as

determined by thermogravimetric analysis due to the torrefaction pretreatment, but the torrefaction increased char yield and char particle density.

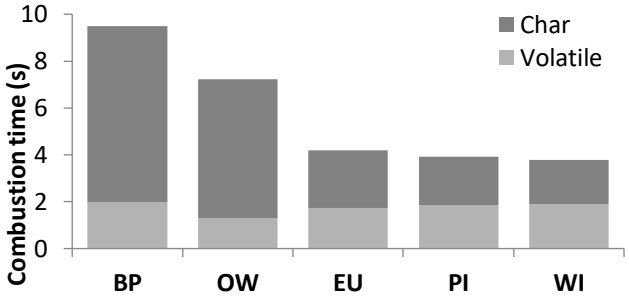

Figure 4. Average burnout time obtained for a 2 mg particle of the different biomass samples.

The average volatile/char time ratio remained constant along the range of particle sizes tried (1-5 mg) for all samples. For the biomass samples EU, PI and WI, the volatile pyrolisis and burnout time was practically equal to the char burnout time. These three samples showed similar times for volatile burning, aligned with very little differences on volatile matter content from the proximate analysis. The volatiles combustion times account for 40 to 50 % over the total combustion time, which is clearly distinctive to OW and BP that account 18 to 20 % on average. This is partially correlated with volatile matter content obtained on the proximate analysis that ranges 80.8-82.5 %, as it can be seen on Figure 5. Olive waste shows a shorter volatile burnout time, as expected due to lower volatile matter content from proximate analysis (74%). Torrefied pellet has a 78% volatile matter on proximate analysis, however the burnout time is slightly higher than the higher volatile matter biomass but the main difference is on the char burnout time, that may be attributed to low fuel reactivity.

Particle density is significative higher on both OW and BP, this has a worsening effect on the heat transfer from the mesh to the particle that could also delay the pyrolysis and char combustion reaction.

The correlation between parameters from proximate analysis, such as volatile content or fixed carbon is not enough to predict burnout times for volatile matter or char combustion times, reflecting the complexity of combustion process on pyrolysis and combustion kinetics.

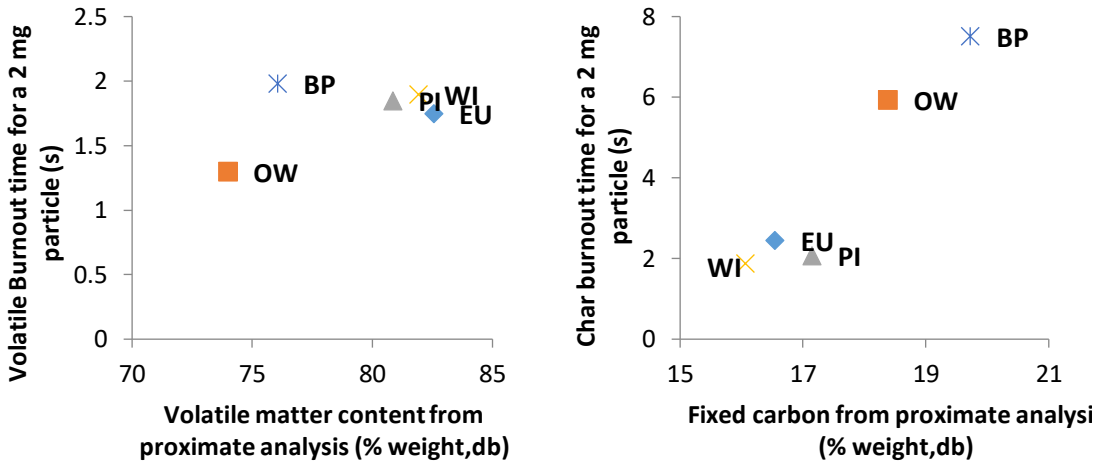

Figure 5. Burnout time for volatiles (a) and char (b) for a 2 mg particle of the different biomass samples versus volatile matter and fixed carbon from proximate analysis respectively.

Particle size distribution and milling process is important for an efficient combustion of fuels. This is especially important on fuels with low reactivity. However for biomass with high reactivity, the burnout time exhibits a lower variation with particle weight or size. This would allow the fuel processing system to be more flexible on its outcome and have less milling energy requirements. In those cases, other parameters such as moisture could be as relevant as the particle size.

3.3. Thermal imaging

The single particle combustion experiment was performed also using a thermal imaging camera instead of the high-speed camera. The experiments were done for three of the samples: PI, EU, WI. Images were obtained through the entire combustion process for a

number of particles of each sample. An example image is presented in figure 6. The surface temperature of the particles was subsequently extracted from the image data and the results are presented in figure 7.

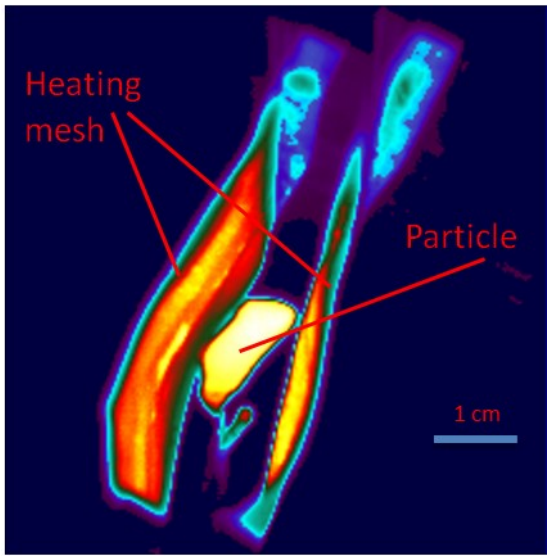

Figure 6 – Thermographic image of particle of EU biomass in wire-mesh reactor

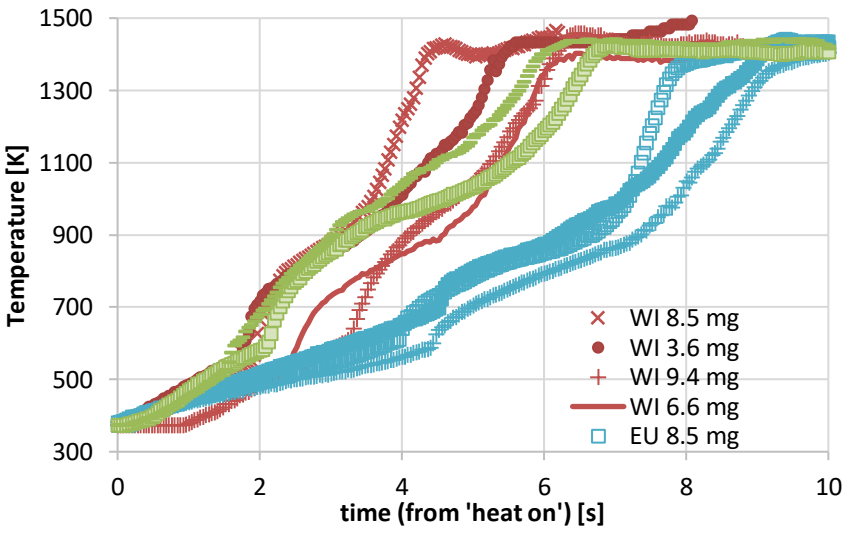

Figure 7 . Surface temperature time-history profile of combusting particles of PI, WI and EU derived from thermal imaging.

379 The surface temperature profile for a number of particles of PI, WI and EU samples is
380 presented in Figure 4. After start heating, the particle surface temperature raises up relatively
381 slow until volatile ignition. Two main increments of the heating rate are observed on the
382 temperature-time profile, corresponding with two changes on slope trend. First notable
383 increment of the surface heating rate is observed when the volatiles ignite with surface
384 temperatures in the range of 500 to 600 K. Pine particles seem to develop a slower heating
385 rate on the surface of the particle. The surface temperature continues increasing on a slower
386 heating rate after volatile ignition. Second increase of the heating rate is related with char
387 ignition, with temperature raising fast until reaching a plateau at a temperature on the range
388 of 1390- 1430 K. Average plateau temperatures for the three samples tested are listed in
389 Table 2. No significative differences were observed among the biomass samples on the
390 plateau temperature during char combustion.
391
392 **3.4. Shape change during particle combustion**
393 No regular behaviour was detected for all particles on their shape and size evolution during
394 combustion. Despite similar origin, shape, size and conditions, different behaviors were
395 observed on the particles of each fuel. In some aspects, even opposite trends were observed
396 as, for example, some particles swell and some shrink at the pyrolysis stage.
397 Length and width dimensions of the particle where recorded at different stages of
398 combustion. A proportional decrease of the particle size would be initially expected during
399 the char combustion. However, this is not what was observed for these samples. As the char
400 combustion progresses the particles instead become more rounded. The shape of the particles
401 with higher aspect ratios changes from a fibrous shape to an ellipsoid that appears to be
402 consumed only in the direction of the length. During volatile flame combustion the particle
403 was not visible at all due to flame screening, however measurements on particle size before

404 ignition and during char combustion where relatively straightforward to take from the video
405 frames. In order to facilitate the comparison among the particles and samples, combustion
406 time, normalized to 100% of total burnout time, for each particle was used. The aspect ratio
407 defined as the length divided by width was also calculated at the different stages of
408 combustion. Some particles were observed to bend over themselves and therefore had to be
409 discarded for the aspect ratio analysis. Some particles were cut manually so the initial
410 dimensions do not necessarily represent the dimensions coming from an industrial mill. The
411 aspect ratio however is on the range of values that would be expected on a large scale milling.
412 Initial aspect ratio for EU, PI and WI were higher than BP and much higher than OW.
413
414 The sample of pine biomass (PI) used had the largest aspect ratio of the samples tried with an
415 initial value of 5.96. No swelling was observed on the vast majority of PI particles. After
416 devolatilization most of the particles shrink slightly on their length, keeping normally the
417 same width as the initial particle. So the aspect ratio of the char obtained after devolatilization
418 was close to the size of the initial particle or slightly lower. During the char combustion
419 stage, the particles are consumed mainly on the tips, while the observed width of the particle
420 remains on similar values as the initial particle until well advanced burnout times. Therefore
421 the aspect ratio of the particle reduces due to length reduction of the burning char. Figure 8
422 represents the average observed aspect ratio of PI particles as well as the standard deviation
423 versus the normalized burnout time.

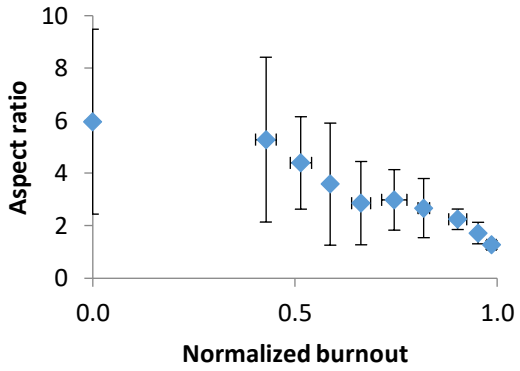

424

425 **Figure 8. Evolution of the average aspect ratio during combustion of PI particles.**

426

427 EU particles had an initial aspect ratio of 4.7, large differences are observed between length
428 and width. A few representative particles of the evolution of the dimensions of EU particles
429 are represented on Figure 9 (length) and Figure 10 (width). On the length the particles
430 observed gradually decrease on size, the dimension evolution on the largest size of the
431 particle generally trend to an asymptotic tendency towards a value around the width.

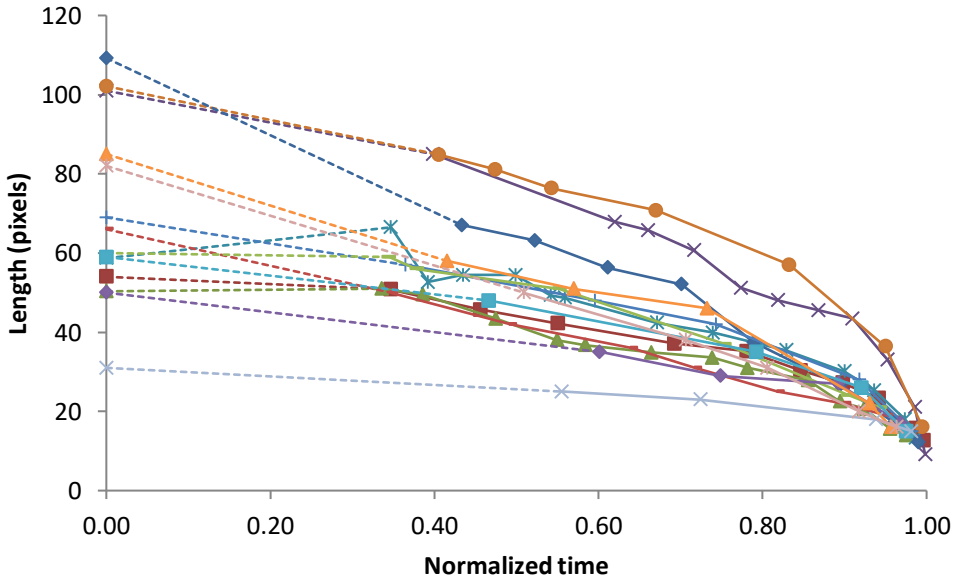

432

433 **Figure 9. Evolution of the length measurements during combustion for various EU**
434 **particles.**

435

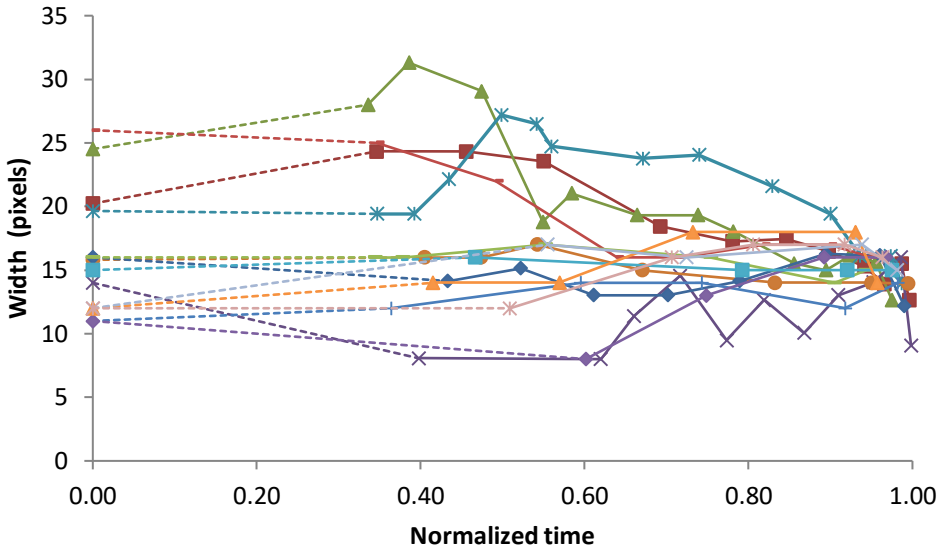

436

437 **Figure 10. Evolution of the width measurements during combustion for various EU**
438 **particles.**

439 Diverse behavior is observed on the width, some particles present apparent swelling while
440 others remain constant or decrease slightly. Those particles that swell during the first step of
441 volatile release, decrease shortly after the ignition of the char surface. The swelling of the
442 particle create a rapid enlargement of the particle dimension. The surface area and higher
443 particle volume created reduces the density considerably. Therefore, once ignited, the char
444 surface is rapidly consumed by the combustion reactions, which explains the fast change on
445 the width on the particles that swell during the volatile combustion. Some particles showed
446 swelling during different stages of combustion. Some particles showed swelling during the
447 first stages of char burning. This could be associated with a higher temperature of the particle
448 during char combustion compared to volatile combustion stage [8] and therefore a softening
449 of the particle while pyrolysis reactions continue occurring inside the particle during char
450 combustion. Particles presenting swelling are generally observed to have slightly shorter
451 burnout time than the average.

452

WI particles did not show significant swelling. The particles shrink gradually on their length on the second half of the char combustion. As observed in the videos, the particle dimension on the width remains constant during the combustion until very end of the combustion (over 95% burnout).

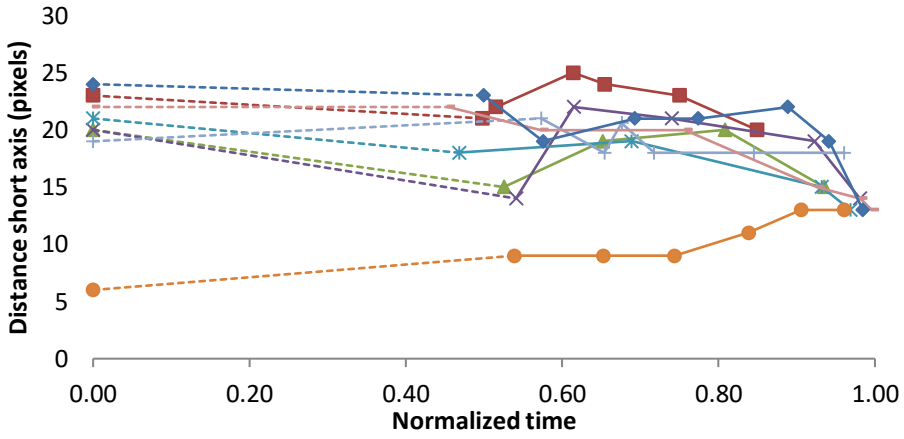

Figure 11. Evolution of the width measurements during combustion of various WI particles.

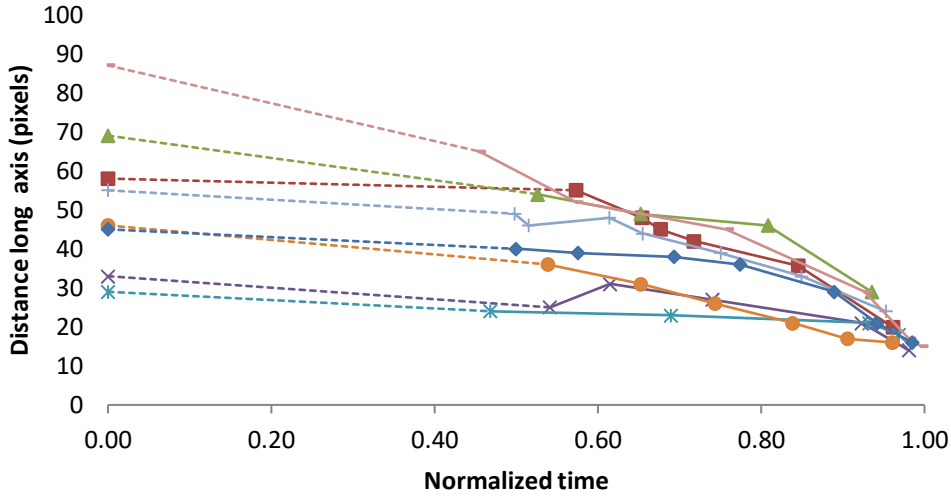

Figure 12. Evolution of the length measurements during combustion of various WI particles.

Neither WI nor PI samples showed any swelling. A slight decrease in the length was observed on the willow particles after devolatilization stage that on average takes half of the total burnout time. No evidence was seen for particle shape changes during the volatile combustion stage for willow sample.

It is notable that particle width remains practically constant during combustion, even increasing in some particles. This increase does not fit on the trend of a swelling particle, and is more likely due to partial melting and spherification process. This was observed by Panahi et al. [21], where much longer and thinner particles were observed to fuse and bend over themselves leading to a almost round char. The different initial aspect ratio on the samples tried in this study and [21] indicates that thin and long particles seem to have higher propensity to spherification during the pyrolysis stage, although this process is not observed for all samples.

The olive waste has been extensively pressed in order to extract the oil so the raw particles are quite round with initial aspect ratio of 1.3±0.36. Differences on the dimensions of width and length were small. The size of the particle is reduced during combustion, however it doesn´t decrease proportionally during time. Particles remain on proportionally large until almost the end of the combustion. At 90% of the combustion time, some particles remain with similar volumes, while some have been reduced to half and others are even larger due to particle swelling. The volatile flame stage is much shorter on the olive waste sample. It was noted that some particles showed swelling during char combustion stage. As previously described for the EU sample, a rapid swelling on the pyrolysis stage is normally followed by a quicker consumption of the particle and a large decrease in particle size shortly after the swelling. This was also the case in a few OW particles, as represented in Figure 13. Both OW

and BP present a high particle density and more compact structure and much lower aspect ratio than the rest of the samples. As described by Biagini et al [34], woody biomass samples present more particles with a fibrous structure that is likely to shrink and fragment. While dense particles with a compact structure are expected to experience minor variations in size

Particles presenting thin aspect do not decrease in size on the short edge size during combustion. This observation was noted on all the samples studied. As observed in Figures 11 and 13, particles with initial small width, remain constant or decrease during combustion and end with very similar width dimensions as the initial particle.

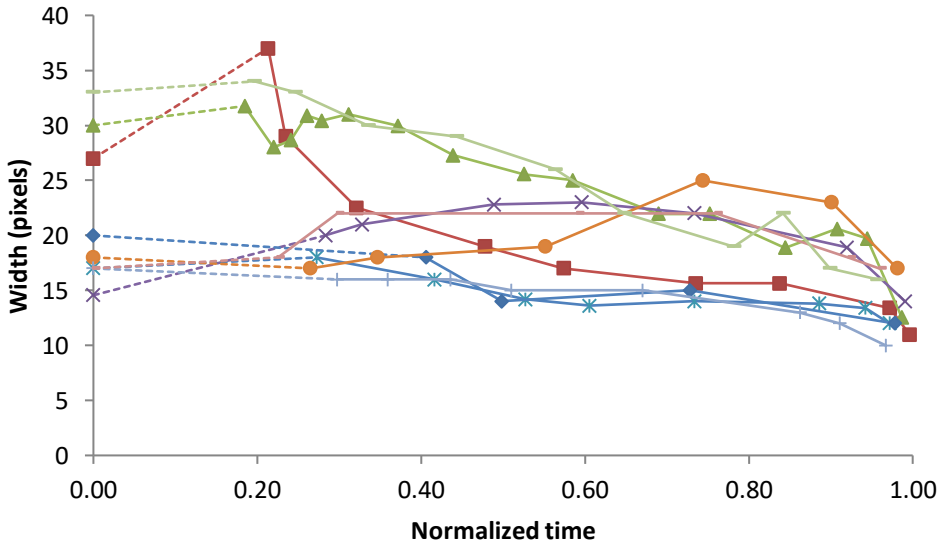

Figure 13. Evolution of the width measurements during combustion of various OW particles.

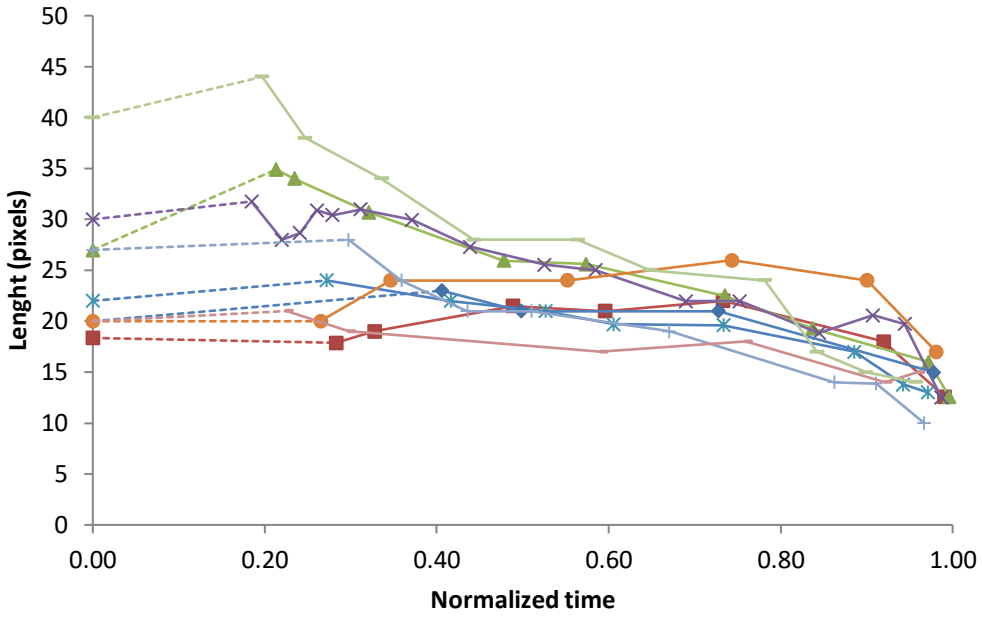

503

504 **Figure 14. Evolution of the length measurements during combustion of various olive**
505 **waste particles.**

506

507 Torrefaction tends to make biomass particles brittle [35]. So, during the processes of milling,
508 pelletization and pellet milling, the particles break, resulting in a lower aspect ratio than a
509 non-torrefied biomass fuel. The fuel sample from the steam-exploded wood pellets reflects
510 this brittleness with an initial average aspect ratio of 1.8, which is low for a woody biomass.
511 The aspect ratio evolution reflects a tendency for the particles to become more rounded at
512 early stages of char combustion. Figure 14 represents the average aspect ratio of the different
513 samples examined. During the volatiles combustion stage the particle was not completely
514 visible and the measurements could not be taken, so the linear evolution assumed during that
515 time is represented with dotted line.

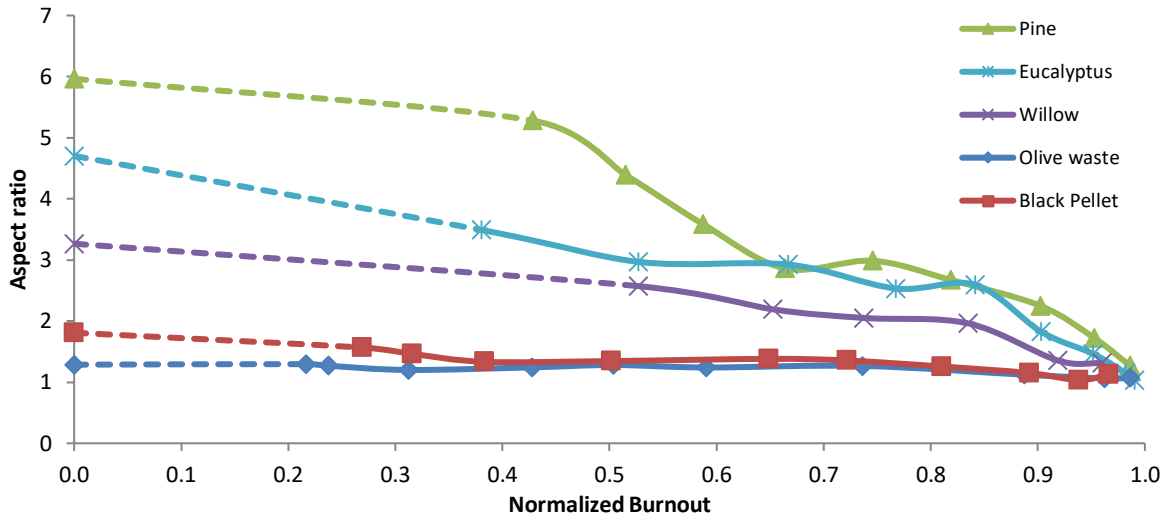

Figure 15. Evolution of the average aspect ratio of all samples during combustion.

Particle density is a key factor during combustion process. The samples with higher particle density tried were OW and BP. These samples presented very small aspect ratios compared to the rest of the samples, with close valued for width and length. The projected areas even increase slightly during pyrolysis and sometimes during char combustion as well, as observed average measurements on Figure 16. The char density has been previously reported to change dramatically during combustion [30], not only due to pyrolysis but also due to the combustion process on the char surface. The heterogeneous combustion reactions take place all over the porous surface of the char and as progresses the oxygen reaches areas closer to the particle centre. Thus the particle volume does not decrease proportionally to the combustion rate. As observed from the projected area on the images, the particles with well advanced combustion rates still have relatively large volumes. Projected area has been calculated assuming the particles as ellipsoids, The equations for the projected area for normalized area of the different samples are listed on Table 2, Regression lines of 2^{nd} and 3^{th} order polynomial have been selected for best fit on each case according to R^2 values,

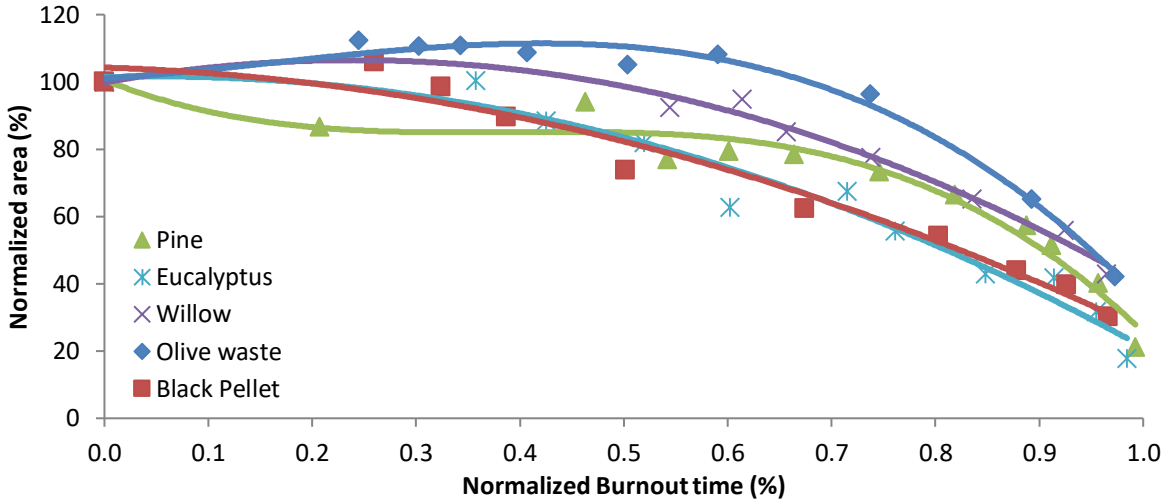

Figure 16. Evolution of the normalized projected area during combustion.

Li and Zang [36] developed a model for combustion of spherical particles that predicts the particle shrinking during the char combustion. The model demonstrated that char consumption is not uniform on the particle surface, being higher at the semi-major axis than at the semi-minor axis. This leads to a decrease in the ellipsoidal particle size. The shape of the particle has been also modelled in previous works, such as Yang et al [22], this works describe with detail a model for a single particle combustion comparing shapes such as sphere and cylinder. The combustion rate on the tip of the cylinder shape is predicted to be higher due to the thinner boundary layer of the reactions front wave. Gradually the particle is assumed to become more round due to higher combustion rate on the thermally thinner parts of the particle. The observations on the particle shape from the videos of the combustion experiments presented in this study do not match with a regular shrinkage. The changes on the shape cannot be only attributed to a higher combustion rate on the tips of elongated particles. This is due to two main observations: first, some particles preserve or even enlarge their width during combustion; secondly the length of the particle shrinks on an irregular rate, accelerating by the end of combustion. This second observation can be attributed to the progressive reduction of the density of the particle. As the biomass char mass is consumed in

552 the combustion process it becomes lighter. The projected area does not reflect a linear
553 reduction during combustion time. As the width of the particles remains practically constant
554 until the end of combustion, the projected area is directly linked with the length of the
555 particle. This relation is stronger for more elongated particles. At the end of the combustion,
556 with 90% burnout the particles are generally equant in width and length. This observation is
557 in agreement with other works such as [37], where the wood particles were observed to
558 change shape looking like droplets at the end of pyrolysis at 1573 K on a drop tube reactor.
559 The projected area then remains circular and a final, very quick, reduction of the area is
560 observable after 90-95% burnout until the end. This has been previously observed by
561 Levendis et al. [38] and Khatami et al. [6] and is described as shrinking core combustion
562 behavior by Shan et al [39].
563 Particle temperature recorded with the thermal camera on the range of 1200-1400 K is
564 enough for melting of the main components of biomass (cellulose and hemicellulose). The
565 melting is likely to happen close to the surface, were combustion takes place and
566 temperatures are high, however the heat transfer between the surface and the centre of the
567 particle is slower than the combustion reaction and prevents the particle to become
568 completely melted under the conditions of this study. Mineral matter among the biomass can
569 play a role in char softening and shape changes, inorganic elements could be spread through
570 the biomass material, and as would be in the particles. Some elements such as Mg, P or K are
571 present in higher concentration in agricultural residues and can decrease the melting point of
572 the ash due to eutectic melting points. Proximate analysis on the different biomass shows
573 high ash content on olive (7.2%), and steam exploded pellet (3.9%) being low in willow and
574 pine (1.8% both) and very low (0.8%) in Eucalyptus. All of them showed shape
575 transformation at different steps of the combustion

576 The temperatures recorded during combustion can be enough to melt certain elements of the
577 ash by mid to end of combustion, as normally ash deformation temperatures for some
578 biomass, can start at 1200 k for biomass rich in K, being higher for those rich in Si or Ca.
579 However the main constituent will be organic material and therefore the main effect this
580 inorganic elements is the catalytic effect that can take part during pyrolysis. Some inorganic
581 elements will catalyze the pyrolysis reactions, accelerating the cracking reactions and
582 allowing the char to get plasticity at low temperatures.
583 Relatively low temperatures have been proven enough to part-melt biomass char compounds
584 as bituminous coals. Trubetskaya et al. [40] observed softening of the solid char matrix
585 already at 350 °C, being greater with increasing temperature and heating rate. This
586 temperature is far below the normal range of ash deformation temperatures. This can explain
587 the slight increase on the width of OR at early stages of the combustion, when temperatures
588 are not expected to be enough to melt main biomass initial constituents.
589 Some particles with prolate shape showed an irregular shape change in various stages. As it
590 can be observed in figure 15 for all samples and particularly for pine in figure 8, the aspect
591 ratio does not decrease following a linear regression. This can be explained due to the
592 different temperature on the out layer of the particle, allowing the particle to deform in the
593 more exposed areas
594 On a first stage the tips get rounded, decreasing the aspect ratio. However the inner structure
595 of the char at the center of the particle remains at lower temperature keeping the particle on
596 an ellipsoid shape until the combustion is well advanced. At the end of combustion, the
597 temperature gradient is negligible and the whole particle is at enough temperature to allow
598 plastic deformation to an almost spherical shape.
599 Surface tension of melted components of the char particle can play an important role on the
600 conformation of particle shape leading to a more rounded particle. This effect is stronger at

601 the end of combustion when particle has been heated for longer times and the combustion
602 front wave has reached the particle centre. Temperature gradient inside the particle will be
603 then negligible and high temperatures, close to the temperature measured on surface are
604 expected at the entire particle.
605
606 **4. Conclusions**
607 All samples presented homogeneous ignition and sequential burning of volatiles and char. BP
608 and OW had shorter volatile burning time, and longer char and total burnout times, .PI, EU,
609 WI were very close to each other with the half of total burnout time of BP. Temperatures
610 measured with the thermal imaging camera for PI, EU, WI show a plateau during char
611 combustion on the range of 1390-1430 K, with no significative differences among the
612 samples. The observed evolution of the dimensions of the particles differs from the gradually
613 reduction on size that would be initially expected. Little changes on the shape and size were
614 observed after the pyrolysis stage. Nor WI nor PI samples presented any swelling, while
615 some particles of OW presented slight swelling in some cases during pyrolysis or char
616 combustion stages. During char combustion the particles become more round. The shape of
617 the particles with initial fibrous shape, changes to an ellipsoid that apparently seems to be
618 consumed only in the direction of the major axis. During char combustion process, long
619 fibrous particles reduce their length, while the observed width of the particle remains on
620 similar values as the initial particle until well advanced burnout times. The projected area of
621 the char particles with well advanced combustion rates still have relatively large values. At
622 the end of the combustion, with 90% burnout the particles are generally equant in width and
623 length. Partial melting of the particle during char combustion allows the surface tension to
624 modify the particle shape, leading to a more round particle. The projected area then remains

as a circle and finally a very quick reduction of the area is observable after 90-95% burnout until the end.

Acknowledgements

The scientific work has been supported by the BIO-CAP-UK project supported by EPSRC thorough the UK CCS Research Centre, www.ukccsrc.ac.uk (UKCCSRC-C1-40) and Supergen Bioenergy Hub. Funding is also acknowledge to the Future Conventional Power research consortium (EP/K02115X/1) supported by The Engineering and Physical Sciences Research Council (EPSRC) (www.epsrc.ac.uk).

Supplementary material

Video files are provided as supplementary material associated with this article and can be found in the online version research data repository Mendeley Data.

References

[1] Ruiz D, San Miguel G, Corona B, López FR. LCA of a multifunctional bioenergy chain based on pellet production. Fuel 2018; 215:601-611

[2] Riaza J, Ajmi M, Gibbins J, Chalmers H. Ignition and Combustion of Single Particles of Coal and Biomass under O_2/CO_2 Atmospheres. Energy Procedia (2017), 114, pag. 6067

[3] Mason PE, Darvell LI, Jones JM, Pourkashanian M, Williams A. Single particle flame-combustion studies on solid biomass fuels. Fuel 2015; 151:21.

[4] Marek E, Stańczyk K. Case studies investigating single coal particle ignition and combustion. Journal of Sustainable Mining 2013;12:17.

[5] Flower M, Gibbins J. A radiant heating wire mesh single-particle biomass combustion apparatus. Fuel (2009), 88, pag. 2418.

650 [6] Khatami R, Stivers C, Joshi K, Levendis Y, Sarofim F. Combustion behavior of single
651 particles from three different coal ranks and from sugar cane bagasse in O_2/N_2 and O_2/CO_2
652 atmospheres. Combust Flame (2012), 159, pag. 1253.
653 [7] Riaza J, Gibbins J, Chalmers H. Ignition and combustion of single particles of coal and
654 biomass. Fuel (2017), 202, pag. 650.
655 [8] Mock C, Lee H, Choi S, Manovic V. Combustion Behavior of Relatively Large
656 Pulverized Biomass Particles at Rapid Heating Rates. Energy and Fuels 2016;30:10809-
657 10822
658 [8] Riaza J, Khatami R, Levendis YA, Álvarez L, Gil MV, Pevida C, et al. Combustion
659 of single biomass particles in air and in oxy-fuel conditions. Biomass Bioenergy
660 2014;64:162–174.
661 [9] Shan L, Kong M, Bennet TD, Sarroza AC, Eastwick C, Sun D,Lu G, Yan Y, Liu H.
662 Studies on combustion behaviours of single biomass particles using a visualization method.
663 Biomass and Bioenergy 2018;109:54-60
664 [10] Carvalho A, Rabaçal M, Costa M, Alzueta MU, Abián M. Effects of potassium and
665 calcium on the early stages of combustion of single biomass particles. Fuel
666 2017;209:787-794
667 [11] Simões G, Magalhães D, Rabaçal M, Costa M. Effect of gas temperature and oxygen
668 concentration on single particle ignition behavior of biomass fuels. Proceedings of the
669 Combustion Institute 2017;36:2235-2242
670 [12] Lu Z, Jian J, Arendt Jensen P, Wu H, Glarborg P. Impact of KCl impregnation on
671 single particle combustion of wood and torrefied wood Fuel 2017;206:684-689
672 [13] Magalhães D, Kazanç F, Ferreira A, Rabaçal M, Costa M. Ignition behavior of
673 Turkish biomass and lignite fuels at low and high heating rates. Fuel 2017:207:154-164

674 [14] Lee H, Choi S. Volatile flame visualization of single pulverized fuel particles.
675 Powder Technology Volume 2018; 333: 353-363
676 [15] Schiemann M, Haarmann S, Vorobiev N. Char burning kinetics from imaging
677 pyrometry: Particle shape effects. Fuel 2014;134:53-62.
678 [16] Biagini E, Narducci P, Tognotti L. Size and structural characterization of lignin-
679 cellulosic fuels after the rapid devolatilization. Fuel 2008;87:177–186
680 [17] Lei K, Ye B, Cao J, Zhang R, Liu D. Combustion characteristics of single particles
681 from bituminous coal and pine sawdust in O2/N2, O2/CO2, and O2/H2O atmospheres.
682 Energies 2017;10:1695
683 [18] Riaza J, Khatami R, Levendis YA, Álvarez L, Gil MV, Pevida C, et al. Single particle
684 ignition and combustion of anthracite, semi-anthracite and bituminous coals in air and
685 simulated oxy-fuel conditions Combustion and Flame 2014,161:1096-1108
686 [19] Zahirović S, Scharler R , Kilpinen P, Obernberger I. Validation of flow simulation
687 and gas combustion sub-models for the CFD-based prediction of NOx formation in biomass
688 grate furnaces. Combustion Theory and Modelling 2010;15: 61-87
689 [20] Bonefacic I, Frankovic B, Kazagic A. Cylindrical particle modelling in pulverized
690 coal and biomass co-firing process. Applied Thermal Engineering 2015;78:74-81
691 [21] Panahi A, Levendis YA, Vorobiev N, Schiemann M. Direct observations on the
692 combustion characteristics of Miscanthus and Beechwood biomass including fusion and
693 spherodization. Fuel Processing Technology 2017;166:41-49
694 [22] Yang Y, Sharifi VN, Swithenbank J, Ma L, Darvell L, Jones JM, Pourkashanian P,
695 Williams A. Combustion of a Single Particle of Biomass. Energy & Fuels 2008; 22:306–316
696 [23] Gubba SR, Ma L, Pourkashanian M, Williams A. Influence of particle shape and
697 internal thermal gradients of biomass particles on pulverised coal/biomass co-fired flames.
698 Fuel Process Technol 2011;92:2185–95.

699 [24] Momeni M, Yin C, Knudsen Kær S, Hvid SL. Comprehensive study of ignition and
700 combustion of single wooden particles. Energy & Fuels 2013;27:1061-1072
701 [25] Lu H, Ip E, Scott J, Foster P, Vickers M, Baxter LL. Effects of particle shape and size
702 on devolatilization of biomass particle. Fuel 2010;89:1156-1168
703 [26] Farazi S, Sadr M, Kang S, Schiemann M, Vorobiev N, Scherer, V, Pitsch H. Resolved
704 simulations of single char particle combustion in a laminar flow field. Fuel 2017;201:15-28
705 [27] Maffei T, Khatami R, Pierucci S, Faravelli T, Ranzi E, Levendis YA. Experimental
706 and modeling study of single coal particle combustion in O2/N2 and Oxy-fuel (O2/CO2)
707 atmospheres. Combustion and Flame 2013;160: 2559-2572
708 [28] Jones JM, Mason PE, Williams A. A compilation of data on the radiant emissivity of
709 some materials at high temperatures, Journal of the Energy Institute, 2018 (in press)
710
711 [29] Magalhães D, Kazanç F, Riaza J, Erensoy S, Kabaklı O Chalmers H. Combustion of
712 Turkish lignites and olive residue: Experiments and kinetic modeling. Fuel 2017;203:868-876
713 [30] Gil MV, Riaza J, Álvarez L, Pevida C, Rubiera F. Biomass devolatilization at high
714 temperature under N2 and CO2: Char morphology and reactivity. Energy 2015;91:655-662
715 [31] Jones JM, Bridgeman TG, Darvell LI, Gudka B, Saddawi A, Williams A. Combustion
716 properties of torrefied willow compared with bituminous coals. Fuel Processing Technology
717 2012;101:1-9
718 [32] Vorobiev N, Becker A, Kruggel-Emden H, Panahi A, Levendis YA, Schiemann M.
719 Particle shape and Stefan flow effects on the burning rate of torrefied biomass. Fuel
720 2017;210:107-120
721 [33] Lu Z, Jian J, Jensen PA, Wu H, Glarborg P. Influence of Torrefaction on Single
722 Particle Combustion of Wood.Energy and Fuels 2016;30:5772-5778

723 [34] Biagini E, Narducci P, Tognotti L. Size and structural characterization of lignin-
724 cellulosic fuels after the rapid devolatilization. Fuel 2008;87:177–186

725 [35] Arias B, Pevida C, Fermoso J, Plaza MG, Rubiera F, Pis JJ. Influence of torrefaction
726 on the grindability and reactivity of woody biomass. Fuel Processing Technology 2008;
727 89:169-175

728 [36] Li J, Zhang J. A theoretical study on char combustion of ellipsoidal particles. ()
729 Combustion Science and Technology 2016;188:40-54

730 [37] Tolvanen H, Kokko L, Raiko R. Fast pyrolysis of coal, peat, and torrefied wood:
731 Mass loss study with a drop-tube reactor, particle geometry analysis, and kinetics modeling.
732 Fuel 2013;111:148-156

733 [38] Levendis Y, Joshi K, Khatami R, Sarofim A. Combustion behavior in air of single
734 particles from three different coal ranks and from sugarcane bagasse. Combust.
735 Flame 2011;158:452-465

736 [39] Shan L, Kong M, Bennet TD, Sarroza AC, Eastwick C, Sun D, Lu G, Yan Y, Liu H.
737 Studies on combustion behaviours of single biomass particles using a visualization method.
738 Biomass and Bioenergy 2018;109:54-60

739 [40] A. Trubetskaya, P.A. Jensen, A.D. Jensen, M. Steibel, H. Spliethoff, P. Glarborg.
740 Influence of fast pyrolysis conditions on yield and structural transformation of biomass chars.
741 Fuel Process Technol, 140 (2015), pp. 205-214

742

743